Geophysical Research Letters

RESEARCH LETTER
10.1029/2020GL090509

Key Points:

- We explored the rapidly evolving controls of postseismic debris remobilization
- The increasing importance of hydrological factors and a large amount of channel deposits cause persisting postseismic debris flow occurrences
- Hazard models need to be frequently updated by timely inventories in order to assess the hazard evolution of postseismic landslides

Supporting Information:

- Supporting Information S1

Correspondence to:

A. P. Yunus and X. Fan,
yunusp@cdut.edu.cn;
fxm_cdut@qq.com

Citation:

Fan, X., Yunus, A. P., Scaringi, G., Catani, F., Siva Subramanian, S., Xu, Q., & Huang, R. (2021). Rapidly evolving controls of landslides after a strong earthquake and implications for hazard assessments. *Geophysical Research Letters*, *48*, e2020GL090509. https://doi.org/10.1029/2020GL090509

Received 28 AUG 2020
Accepted 23 NOV 2020

Author Contributions

X. Fan, A. P. Yunus, and G. Scaringi led the research, formulated the research questions, and defined the manuscript contents in line with discussions with F. Catani, S. Siva Subramanian, Q. Xu, and R. Huang. A. P. Yunus prepared the manuscript, with contributions from X. Fan, G. Scaringi, F. Catani, and S. Siva Subramanian. X. Fan, G. Scaringi, Q. Xu, and R. Huang involved in the compilation of landslide inventory. A. P. Yunus, G. Scaringi, and F. Catani analyzed the background literature and the statistical analysis. A. P. Yunus and F. Catani analyzed the controlling factors and performed the susceptibility assessments. All co-authors revised and approved the manuscript.

Rapidly Evolving Controls of Landslides After a Strong Earthquake and Implications for Hazard Assessments

Xuanmei Fan[1], Ali P. Yunus[1], Gianvito Scaringi[2], Filippo Catani[3], Srikrishnan Siva Subramanian[1], Qiang Xu[1], and Runqui Huang[1]

[1]State Key Laboratory of Geohazard Prevention and Geoenvironment Protection, Chengdu University of Technology, Chengdu, Sichuan, People's Republic of China, [2]Faculty of Science, Institute of Hydrogeology, Engineering Geology and Applied Geophysics, Charles University, Prague, Czech Republic, [3]Department of Geosciences, University of Padova, Padova, Italy

Abstract Strong earthquakes, especially on mountain slopes, can generate large amounts of unconsolidated deposits, prone to remobilization by aftershocks and rainstorms. Assessing the hazard they pose and what drives their movement in the years following the mainshock has not yet been attempted, primarily because multitemporal landslide inventories are lacking. By exploiting a multitemporal inventory (2005–2018) covering the epicentral region of the 2008 Wenchuan Earthquake and a set of conditioning factors (seismic, topographic, and hydrological), we perform statistical tests to understand the temporal evolution of these factors affecting debris remobilizations. Our analyses, supported by a random-forest susceptibility assessment model, reveal a prediction capability of seismic-related variables declining with time, as opposed to hydro-topographic parameters gaining importance and becoming predominant within a decade. These results may have important implications on the way conventional susceptibility/hazard assessment models should be employed in areas where coseismic landslides are the main sediment production mechanism on slopes.

Plain Language Summary Strong earthquakes in mountain regions can trigger thousands of landslides, forming deposits of rock and soil debris along steep slopes. Months to years later, rainstorms may generate debris flows—destructive water-debris mixtures that rush downslope and flood valleys. Scientists use models to estimate the hazard of landslides and debris flows, which are based on accurate maps of the slopes, the type of rock or soil, inventories of known landslides, rainfall trends, and more. Susceptibility and hazard maps are the main product of these models. They are used to predict the probability of a hazardous event occurring at a given location in a given time span. These maps are usually "static," in the sense that they are thought to remain valid for a long time because the data they are based upon (such as the shape of slopes) do not vary much. However, postearthquake landscapes are very dynamic: debris moves downslope, carried by rain or shaken by aftershocks; meanwhile, new landslides occur on some slopes, while others revegetate and stabilize. The overall picture is complex as many variables are involved. We use machine learning to demonstrate that static hazard maps become unable to predict landslides after just a few years, and advocate for the use of frequently updated maps linked to fresh inputs, tracking the location and activity of debris deposits, and old and new landslides.

1. Introduction

Rainfall-induced remobilizations of coseismic landslide deposits, propagating from hillslopes to downstream (Dahlquist & West, 2019), are a typical hazard in areas affected by earthquake-induced landslides (X. Fan et al., 2019a). These deposits are typically constituted by loose materials with significant amounts of fines, hence they are susceptible to sudden collapse and liquefaction upon loss of suction or pore water pressure increase (Hu et al., 2017, 2018). Debris remobilization events may occur in the earthquake-affected areas for years or decades (Hovius et al., 2011; Keefer, 1994; Yunus et al., 2020), even multiple times in the same deposit, largely depending on the volumes of coseismic deposits and rainfall intensities (Dadson et al., 2004; Hovius et al., 1997; Marc et al., 2016). Together with delayed (postseismic) slope failures, they concur to the generation of destructive debris flows, posing an additional threat to areas already hit by the earthquake. Where these remobilizations evolved into debris flows, such as in Wenchuan county (China), they caused human losses and extensive damage to property and infrastructure (Tang et al., 2011; Q. Xu

et al., 2012). Hence, understanding their spatial likelihood and controlling factors is critical for mitigating the risk through proper countermeasures and reconstruction strategies.

A generally accepted assumption in landslide susceptibility/hazard mapping is that the controlling factors do not change significantly over a long period of time; therefore, susceptibility/hazard maps for a given area can be assumed to be static (Segoni et al., 2018). This hypothesis is especially convenient if the susceptibility is derived from landslide inventories that cover a considerable time span, as it simplifies their interpretation. However, high-relief landscapes after a strong earthquake undergo rapid evolution, accompanied by rapid changes in hydro-mechanical properties. Grain size coarsening, increase of permeability, consolidation, and progressive revegetation have indeed been observed in coseismic landslide deposits (Domènech et al., 2019; G. Li et al., 2017; Zhang & Zhang, 2017). Therefore, predicting subsequent debris flows using a static set of factors and weights may not be advisable, and the resulting susceptibility/hazard maps may be unreliable. At present, though, these statements remain unproven, mainly owing to the scarcity of multitemporal inventories tracking debris remobilization occurrences in the years following a strong earthquake. Such inventories are essential for understanding the spatiotemporal patterns of future landslides. To the best of our knowledge, only a few studies have mapped these occurrences systematically in worldwide earthquake cases (Dahlquist & West, 2019; R. L. Fan et al., 2018a; Lin et al., 2004; Shafique, 2020; Shou et al., 2011; Tian et al., 2020), and in limited areas affected by the Wenchuan Earthquake (M. Chen et al., 2020; X. Fan et al., 2019b; Shen et al., 2020; Tang et al., 2016; Yang et al., 2017, 2018), yet no multitemporal postseismic susceptibility and controlling factor assessments have been attempted thus far.

Here, we explore the evolving controls of coseismic landslides and postseismic material remobilizations along the hillslopes following the 2008 Wenchuan Earthquake using a multitemporal landslide inventory of the epicentral region (X. Fan et al., 2018b, 2019b). We assess and rank controlling factors, predict the likelihood of remobilizations, and discuss implications and challenges in hazard assessment procedures.

2. Study Area

The 2008 M_w 7.9 Wenchuan Earthquake triggered an unprecedented number of landslides across the Longmenshan mountain range, generating at least 2–3 km^3 of mass wasting (Li et al., 2018b; C. Xu et al., 2014). Many previous studies concluded that the earthquake-affected area still retains a high geological hazard related to delayed landslides, postseismic debris flows, and severe erosion (Li et al., 2018; Tang et al., 2016; Yang et al., 2018). Coseismic landslide deposits on steep (>40°) hillslopes are more likely to be remobilized and supply material for debris flows during subsequent rainfall events (Zhang & Zhang, 2017). Here, we investigate a portion of the Longmenshan between the Wenchuan-Maowen and Yingxiu-Beichuan faults, where the earthquake rupture initiated (Figure 1).

The study area (471 km^2) is subdivided into 42 catchments with elevations of ~450–4,000 m a.s.l. The climate is subtropical and monsoonal (mean annual temperature: 13°C; precipitation: >1,250 mm/year), with rainfall concentrated in July and August.

3. Data and Methods

Over the past decades, the availability of high-resolution remotely sensed data has led to increasingly complete inventories of coseismic landslides becoming available (Martha et al., 2013; Tang et al., 2016, 2019; van Westen et al., 2008). We used a multitemporal inventory of landslides in the epicentral region of the 2008 Wenchuan Earthquake, produced from pre and postearthquake remote sensing images recorded from 2005 to 2018 (X. Fan et al., 2019b), as it covers the largest area and longest time span for the Wenchuan Earthquake-affected region thus far. The total area of coseismic landslides in these catchments is 72.8 km^2 (Figure 1). Key details of the inventories can be found in Domènech et al. (2018) and in Text S1 (supporting information).

We examined the factors controlling landslide occurrences in the study area. In the literature, no standard guideline exists on the appropriate selection of landslide conditioning factors (LCF). According to

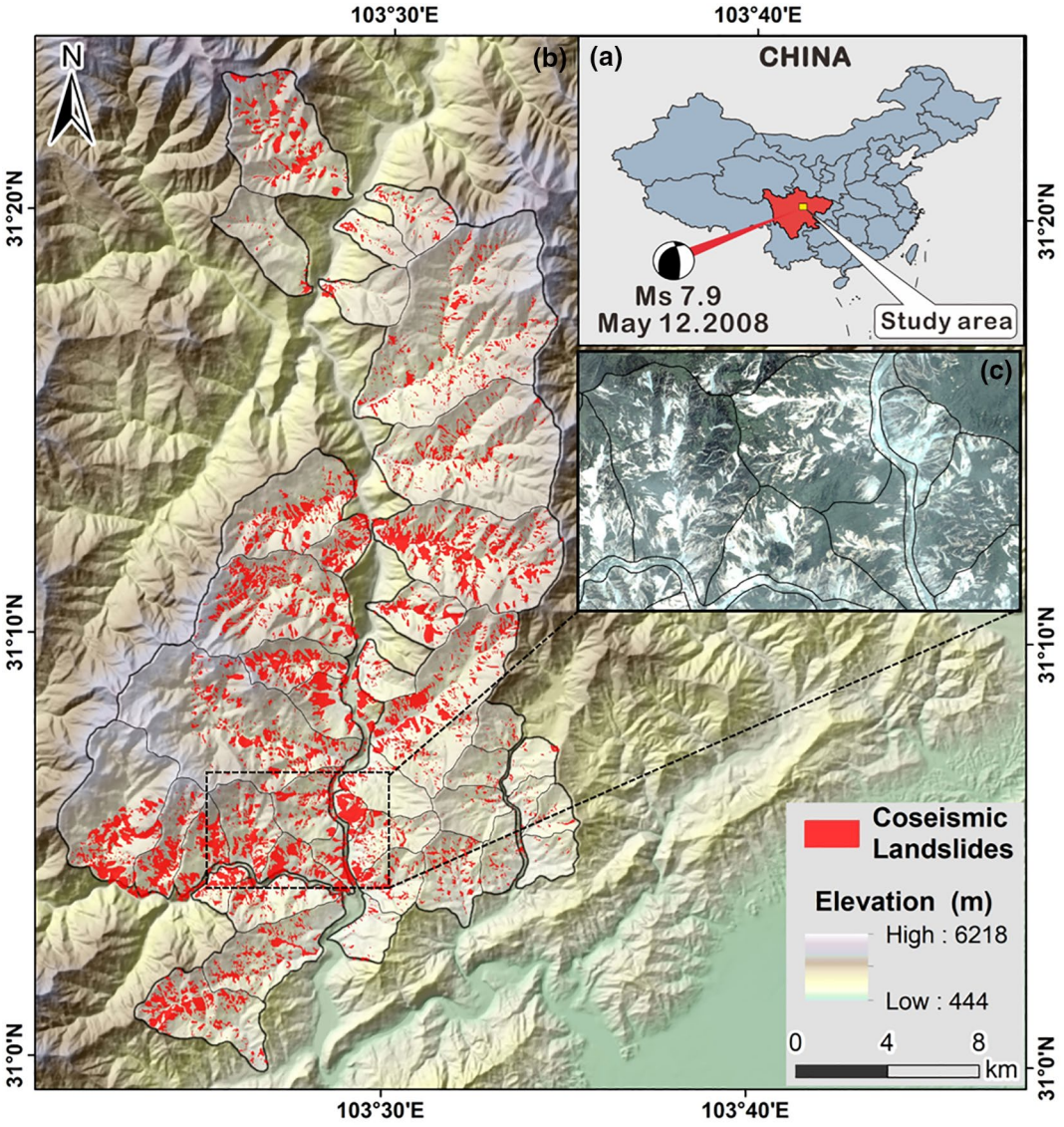

Figure 1. (a) Location of the study area in Sichuan, China; (b) coseismic landslide distribution (Source: Domènech et al., 2018); and (c) inset showing high-resolution satellite imagery (Worldview 2) used for landslide mapping.

Reichenbach et al. (2018), the availability of data pertaining to the study area is often crucial in deciding the selection of LCF. Merghadi et al. (2020) explained a step-by-step procedure for selecting the LCF which involves identifying and selecting all geo-environmental factors available for the study area, followed by collinearity tests and feature selection algorithms. Therefore, we initially selected a large set of independent variables from the literature (lithologic, tectonic, topographic, hydrologic, and seismic factors) that may explain the governing mechanisms and spatial distribution of coseismic landslides (e.g., Carro et al., 2003; Y. Chen et al., 2020; Lee et al., 2008; Nowicki Jessee et al., 2018) as well as of "nonseismic" landslides in our study area (Table 1 and Text S2, supporting information). The distribution and volume of coseismic landslides also may have a significant impact on the distribution of postseismic remobilizations. Hence, the volumes of coseismic and remobilized landslides were also analyzed (Table 1).

Subsequently, we performed a collinearity test to reveal relations among (initially assumed) independent variables. Multicollinearity occurs when a variable is highly correlated with one or more other variables (Allen, 1997). Variance inflation factor (VIF) and tolerance (TOL, i.e., 1/VIF) are two common tests for

Table 1
Conditioning Factors Used in This Study, General Description, and Collinearity Test Results

Type	Landslide conditioning factor	Source, meaning	Collinearity test	
			VIF	*VIF* (after removing MRI, MINT, and AAA)
I	ELE—Elevation	Elevation data taken directly from the 25 m resolution digital elevation	1.76	1.65
	SLO—Slope	Slope angle (in degrees)	2.50	2.20
	ASP—Aspect	Orientation of the slope being the north defined as 0° and 360° and the south 180°	1.10	1.10
	CUR—Planar curvature	Displays the shape or curvature of the slope. Plan curvature relates to the convergence and divergence of flow across a surface	1.96	1.95
	POS—Positive openness	Positive openness expresses surface convexity (Yokoyama et al., 2002)	7667.99	1.00
	MRI—Melton Ruggedness Number	Expresses the relative dynamism of the basin; indicator of hazardousness of the basin (Slaymaker, 2010)	7671.67	REMOVED
	MPI—Morphometric Protection Index	Analyses the immediate surrounding of each cell up to a given distance and evaluates how the relief protects it	5.76	5.63
	TPI—Topographic Position Index	Index of cell position relative to ridges and valleys. Positive TPI = closer to ridges. Negative TPI = closer to valleys. TPI zero = either flat areas or areas of constant slope (Jenness, 2006)	6.28	5.60
II	LITH—Lithology	Categorical code of the main lithological units present in the study area (scale 1:200,000)	1.03	1.02
III	NDVI	Normalized difference vegetation index derived from Landsat 5 TM, 7 ETM, and 8 OLI images	1.009	1.002
IV	FACC—Flow Accumulation	Cumulative hydrologic flow values representing the number of input pixels contributing water to any outlets	1.23	1.23
	DTS—Distance to Stream	Distance from the channel network extracted using 0.4 km^2 as threshold contributing area	1.03	1.03
	RAIN—Rainfall Anomaly	Gridded 25 m resolution map of interpolated rain anomaly using SM2RAIN algorithm (Brocca et al., 2014)	2.42	2.10
	RAIN1—TRMM Rainfall	Gridded 0.25° annual rainfall derived from TRMM for each analyzed year	1.07	1.07
	DAH—Diurnal Anisotropic Heat	Simple approximation of the anisotropic diurnal heat (Ha)	1.07	1.06
V	PGA—Peak Ground Acceleration	Seismic data obtained from the China Earthquake Networks Center (CENC)	6.63	5.28
	PGV—Peak Ground Velocity		10.57	4.87
	MINT—Maximum seismic Intensity		11.14	REMOVED
VI	COS—Volume of Coseismic Deposits	Estimated from postevent satellite images (2008–2018; Domènech et al., 2018). Volume of landslides were calculated based on Larsen et al. (2010) but channelized debris and debris flows were not calculated using area-volume relationships but directly by integrating the area covered by the deposits over the pre-earthquake DEM	1.16	1.14
	VPS—Volume of Active Landslides of Previous Year		1.09	1.09
VII	RAND—Random Variable		1.00	1.00

Types: I—topographic factors, II—lithologic factors, III—vegetation, Type IV—hydro-climatic factors, V—seismic factors, VI—postseismic factors.

collinearity. According to previous studies, VIF > 10 or TOL < 0.1 indicate significant multicollinearity (Dormann et al., 2013; Merghadi et al., 2018). Table 1 summarizes the VIF values for the LCF. Among the factors that exhibited significant multicollinearity, we decided to remove those with the largest VIF value in the further analysis. Therefore, we removed POS but retained MRI, and removed MINT but retained PGV. After removal, a new collinearity test did not evidence issues.

We then analyzed the relative importance of the 18 remaining variables, and a random variable with respect to the explanatory power for postseismic debris remobilizations for each mapped year using the information gain (*IG*) function.

According to Hall and Holmes (2003), *IG* is one of the quick and easiest attribute ranking methods that is often used in feature selections and for identifying root nodes in tree-based models (e.g., Alhaj et al., 2016; Lei, 2012; Quinlan, 1986). Therefore, the attributes providing more information on the dependent variable will have a higher *IG* value. To perform *IG* and later susceptibility model analysis, we randomly selected 50,000 sampling points within the basin area for each analyzed year, including both landslide and nonlandslide pixels. As the number of nonlandslide samples is predominant compared to the number of landslide samples, we also introduced a censoring of nonlandslide samples to avoid data imbalancing. We finally extracted the values of each LCF (Table 1) for each of the selected pixels. The mathematical representation of *IG and a sample calculation*, the reader is referred to Text S3 (supporting information) and Andrews et al. (2007). We calculated *IG* for each LCF in each inventory, before and after the earthquake. A ranking of the IG values was made according to their weights, which we used to study the temporal evolution of the factors.

Finally, we applied a random forest model (RFM) to assess the landslide susceptibility via the 18 selected variables, thereby evaluating changes of predictive power with time. We chose the RFM after exploring various machine-learning alternatives (e.g., logistic regression, decision trees, and K-nearest neighbors), which were all outperformed by the RFM (see Texts S4 and S5, supporting information). Also, since our objective is to compare susceptibility estimations made under evolving controls, we needed to adopt a statistical inference model with a low sensitivity toward changes in the independent variable set. RFM is particularly robust on this regard, provided that the forest of binary trees is dense enough (Catani et al., 2013; Dou et al., 2019; Yunus et al., 2019).

We first trained the RFM using the 2011 inventory data. A 10k-fold cross validation approach was used for validating the models, and a complete set of pixels was used to validate the 2011 model in the subsequent (2013, 2015, and 2017–2018) years. Similarly, susceptibility models were built and validated using the 2013, 2015, and 2017–2018 inventories. The hyperparameters, that is, the number of trees, maximum depth, and the number of predictive variables used to split the nodes in RFM are selected as the default values in WEKA© environment to replicate the results. The model estimated a pixel-based probability of remobilization for the same year and the subsequent ones. For performance evaluation, the confusion matrix, Kappa values, accuracy (ACC), area underneath the receiver operating characteristic (ROC) curve (AUC), and the precision recall area under the curve (PRC) were used (the matrix evaluation is explained in Text S4, supporting information).

4. Results

4.1. Evolving Controls

The conditioning factors, ranked according to their *IG* values, are shown in Figure 2. Consistently with general knowledge on nonseismic landslides, rainfall (rainfall anomaly) exerted the strongest control on landslide occurrence before the earthquake (2005–2007). Topographic variables, such as elevation, slope, aspect, and positive openness also ranked high. Upon the earthquake (2008), however, the importance of the topographic variables remained high, whereas lithology, curvature, and normalized difference vegetation index (NDVI) decreased significantly. The seismic strength indicators, PGA and PGV, did not rank as high as expected. One possible explanation is that PGA and PGV for the Wenchuan Earthquake varied significantly over a spatial scale, in the direction orthogonal to that of the seismogenic fault, which is quite large in comparison with the size of the study area in the same direction. Lithology exerted a weak control owing to the limited variation of lithologies in our study area, which in turn limits the statistical significance. With reference to the whole earthquake-affected area, Gorum et al. (2011) also showed that the effect of lithology was not very clear, whereas the fault mechanism, the hanging wall/footwall effect, and topography controlled the landslide distribution the most. Our study area lies entirely on the hanging wall, and features a rather homogeneous lithology. Another reason for the limited relevance of lithology could be linked to the

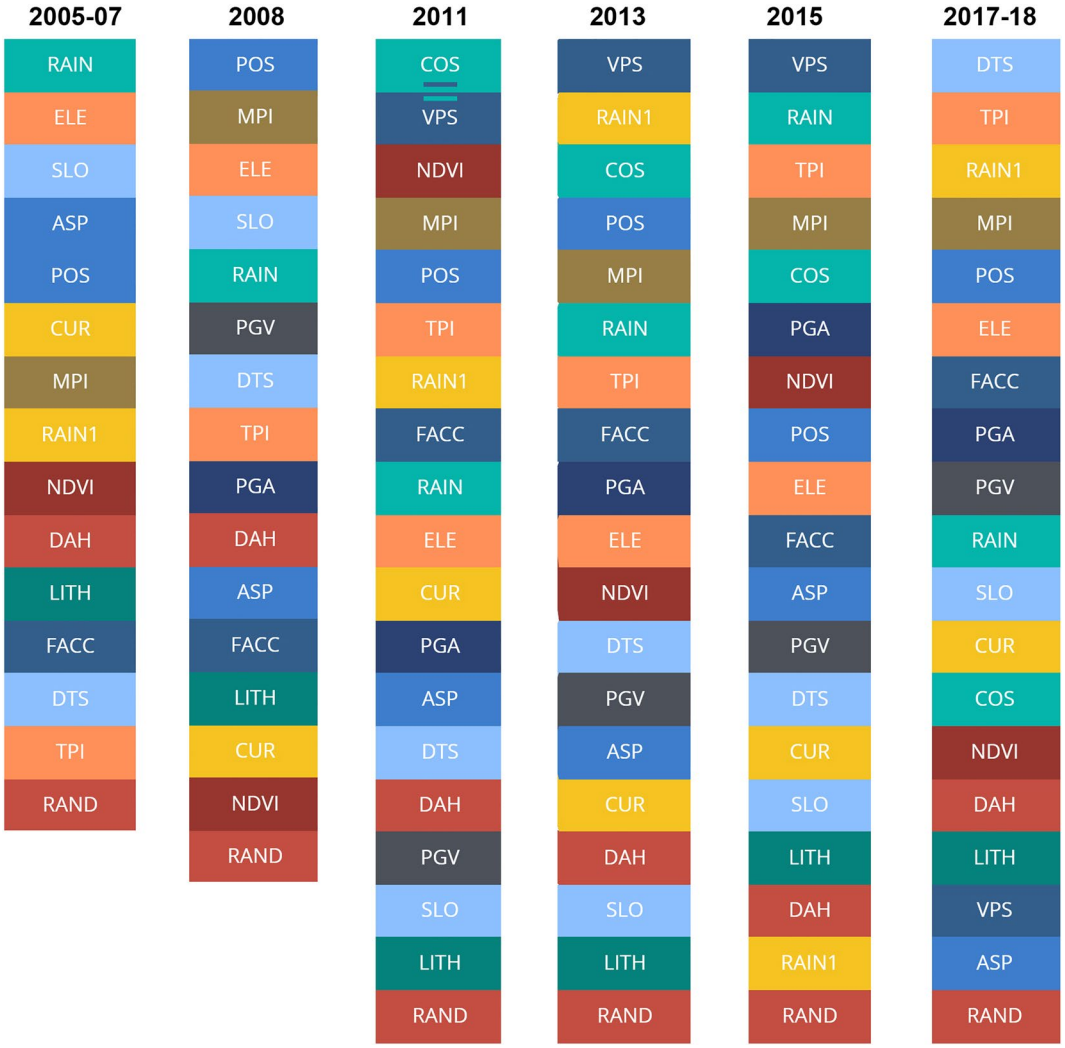

Figure 2. Information gain (IG) ranking (descending order in each column) of conditioning factors obtained for each year (2005–2018).

very nature of the available geological maps, which mostly convey information on the bedrock materials rather than on the regolith cover and the slope deposits that are the main source of material for landslides in the area (Segoni et al., 2020).

In 2011 (Figure 2), the volume of coseismic landslides (COS), NDVI (indicating uprooted vegetation), topographic position (MPI, POS, and TPI), and rainfall (annual) became the main controls. The influence of vegetation on the occurrence of landslides, however, is not a straightforward one in the sense that a low vegetation coverage might contribute to make landslides more likely, but may also be the result of the occurrence of landslides in the immediate past. In the study area, the strong seismic forcing overrode many other factors in determining the occurrence of landslides: areas with deep-rooted arboreal vegetation suffered landslides as much as areas covered with grass or bare land. The relationship between the slope location, as well as topographic factors, were more relevant in determining landslide occurrence than the preearthquake vegetation cover. In the years after the earthquake, the situation changes such that a low NDVI values can signal the locations affected by coseismic landslides. In subsequent years (2013–2015), the volume of previous landslides (VPS), that of coseismic landslides (COS), rainfall (annual) largely determined the remobilizations (Figure 2). Additionally, rainfall anomaly progressively regained importance up to the preearthquake value, which is consistent with the observation that increasingly heavier rainfall

triggered all of the postearthquake debris flows (X. Fan et al., 2019a; Zhang & Zhang, 2017). One can also notice that the PGA has gained significance after the 2011. This is because as time elapses, it is mostly the larger deposits that remain active; these are, in general, associated with stronger shaking and weaker underlying materials. In this sense, these hillslopes carry with them the signature of the earthquake for a comparatively longer time.

Finally, in 2017 and 2018, a limited control of coseismic landslide deposits (COS) and VPS was observed, possibly in response to a progressive depletion of fines from the hillslope deposits (Domènech et al., 2019), which decreases the likelihood of hydrologically triggered instability. Revegetation also was observed (reduced NDVI rank) to play a role in limiting soil erosion, and thus runoff-induced failures (Shen et al., 2020; Yunus et al., 2020). Interestingly, the distance to streams (DTS) became the most important factor, consistently with the higher landslide rates observed in channels and by river sides rather than high on the hillslopes. Confirming this analysis, during a heavy rainfall period in August 2019, catastrophic debris flows occurred in 20 gullies involving an area of 4.72×10^6 m^2 in the study area. The total accumulated rain from August 1st to 20th was 331 mm, much higher than the average for August (250 mm). Noticeably, all the debris flows occurred within tributary channels (see Text S6, supporting information). The topographic position index (TPI) gradually moved toward the top of ranking since 2005, suggesting that the material has moved closer to the streams from the hill-slopes.

These results suggest that, in general, the importance of coseismic variables, initially high, should decrease progressively in favor of nonseismic or postseismic factors within a few years (Figure 2). In turn, this may imply that strong seismic shocks may produce sudden changes in the spatial distribution of mass wasting processes on slopes, by "resetting" slope instability drivers and refilling the sediment storage on hillslopes. These processes would continue until the preearthquake physical parameters are restored, and hence also the controls to mass wasting. This observation may have important implications for mapping and predicting the landslide hazard after strong earthquakes, as will be discussed in the following sections.

4.2. Postseismic Debris Remobilization Susceptibility Assessment

To provide a benchmark on the implications of time-variable controls to hazard prediction, we performed a postseismic debris remobilization susceptibility assessment for the study area using a RFM on randomly sampled pixels (of postseismic remobilizations and nonremobilizations within the coseismic landslide boundaries) from the 2011 inventory maps. The spatial probability of postseismic remobilizations obtained from the RFM for 2011 is shown in Figures 3a–3d. Quantitative assessment of the remobilization susceptibility classes (very low, 0–0.2; low, 0.2–0.4; medium, 0.4–0.6; high, 0.6–0.8; and very high, 0.8–1) assigns 61% of the coseismic deposits to the very low susceptibility class, 24% to the low/medium classes, and 15% to the high/very high classes. The latter cover ~16.44 out of 471 km^2 of the study area, a value very similar to the areas with actual remobilization in 2011 (17.42 km^2), with which they have a statistically significant correlation ($R^2 = 0.89$, $p < 0.01$).

The model performance was evaluated using the confusion matrix, Kappa coefficient, ACC, and area under the ROC curve (AUC). These indicators are presented in Figure 3e. The true positive rate (TPR) and Kappa for the RFM in 2011 (70% and 0.57, respectively) indicate a good predictive performance. The prediction of postseismic landslides in 2013 using the model trained on the 2011 inventory yields lower TPR and Kappa values (43% and 0.41, respectively). Validation of the same model for the 2015 and 2017–2018 inventories yields lower TPR and Kappa values similar to those in 2013, which are unsatisfactory considering that the false negative rate (FPR) exceeds the TPR (Figure 3e). Similarly, susceptibility models were also trained on the 2013 and 2015 inventories, and validated on the same and subsequent inventories (Text S4, supporting information). TPR, FPR, and Kappa values indicate that the models are less successful in predicting future scenarios (Text S4, supporting information).

5. Discussion

Our analysis of statistically derived temporal controls of landslides highlights two prominent mechanisms of postseismic activities: (i) typical topographic controls of landslide such as slope and elevation gained importance and became predominant within a decade (Figure 2), in line with a frequency of new hillslope

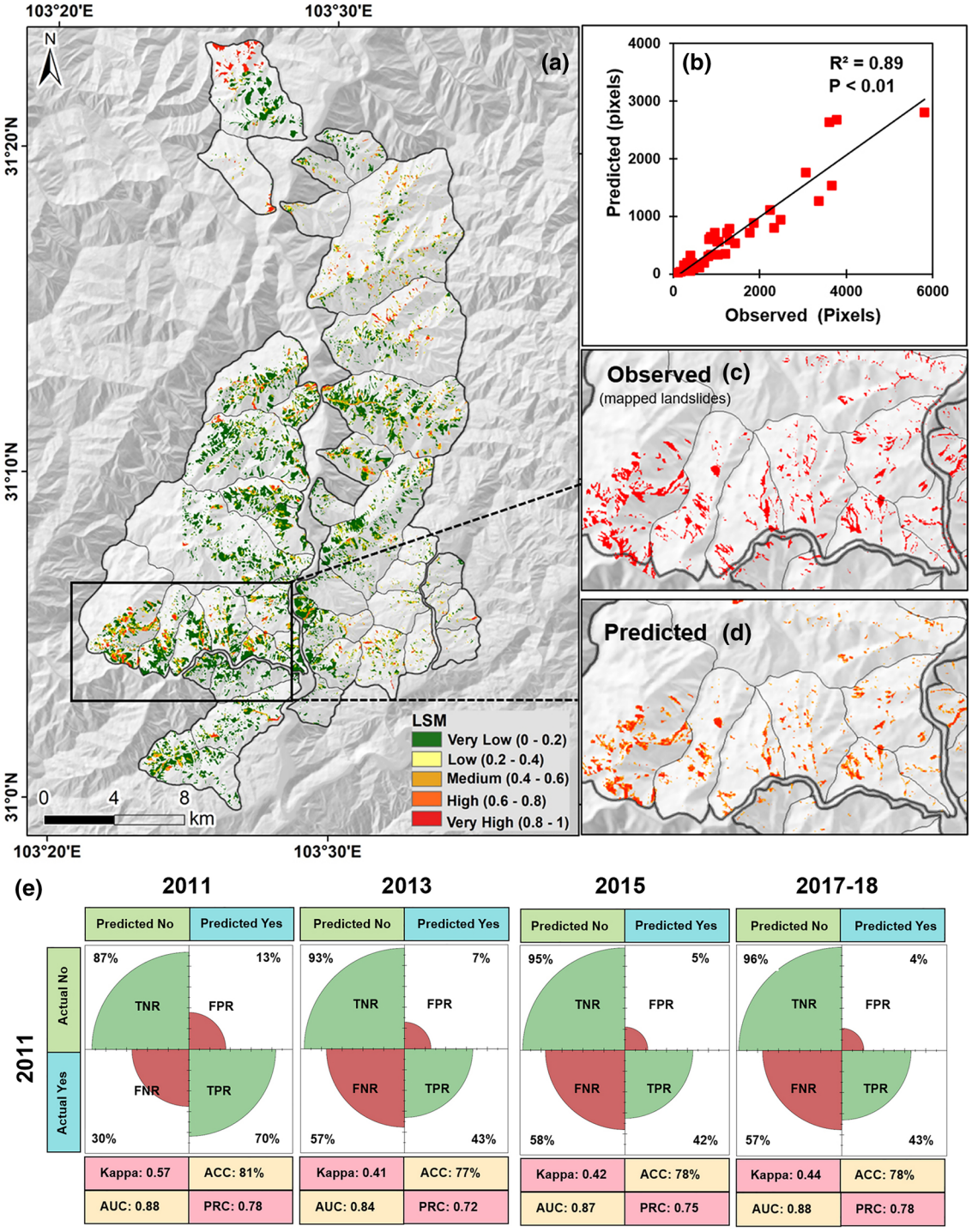

Figure 3. (a–d) Postseismic remobilization susceptibility assessment in the study area in 2011 revealed by a Random Forest model. (e) Performance of susceptibility models trained on landslide inventories from different years evaluated by confusion matrix, Kappa coefficient, accuracy (ACC), area under the ROC curve (AUC), and the precision Recall area under curve (PRC).

failures (hillslope deposit remobilizations) decreasing progressively; (ii) the importance of hydrological factors (DTS and FACC) and topographic position (TPI) has increased since 2008 (Figure 2), indicating that debris materials have moved into or closer to channels (remobilizations are constrained by erosion of channel deposits and debris flows).

The first point is a positive sign in a disaster perspective view. The frequency of postseismic debris remobilizations decreased from 3,549 to less than 100 per year within a decade. This rapid decay is consistent among all recent major earthquakes (Hovius et al., 2011b; Marc et al., 2015; Zhang et al., 2016), and partly constrained the postseismic sediment transport (Wang et al., 2017). In both the Wenchuan and Gorkha regions, researchers argue that most of the loose material generated by earthquake-induced landslides remained confined to hillslopes and tributary channels of catchments, whereas only a minor proportion of it has been evacuated from the catchments thus far (Dahlquist & West, 2019). In Wenchuan, previous studies (X. Fan et al., 2018b, 2019a) indicate that more than 90% of coseismic landslide deposits remained on the mountainous landscapes and became stabilized, possibly as a result of preferential removal of fine sediment and revegetation processes (e.g., Domènech et al., 2019). However, the mechanisms governing the postseismic sediment cascade and the rate at which the remaining sediment is removed from the landslide-impacted regions are unknown, which calls for in-depth research toward a better understanding of landscape evolution in tectonically active mountain ranges (Croissant et al., 2019) over larger time frames.

On the downside, destructive debris flows keep occurring during rainy seasons even a decade after the mainshock because of the increasing coupling between the location of debris deposits and the hydrological controls of remobilizations (see point (ii) above). The latest record is from August 2019, causing 10 fatalities related to debris flows in Wenchuan region (Petley, 2019). An elevated frequency of debris flows has been reported also after the 2015 Gorkha earthquake in Nepal (Dahlquist & West, 2019).

The decreasing frequency of remobilizations of hillslope deposits and the persisting debris flow occurrences, though seemingly inconsistent, are both supported by the rapid evolution of controlling factors, as shown by our analysis. The significant control of the volume of landslide deposits (COS and VPS) and the reduced role of topographic and hydrological factors in the first few years (2008–2015) after the earthquake (Figure 2) imply that remobilizations are triggered almost stochastically wherever there are landslide deposits. This also explains why a static susceptibility model calibrated on a landslide map and factors of a specific year does not perform well when predicting remobilizations in next years. However, through time, a preferential occurrence of remobilizations in deposits closer to channels tends to emerge, reflecting the increasing importance of hydrological factors (Figure 2), which are usually dominant in nonseismic scenarios. Therefore, aiming at risk reduction with a temporal horizon beyond that of the postearthquake emergency response, the focus of attention should shift onto monitoring the loose debris in gully networks.

The rapid change of relative importance among the controlling factors of postseismic landslides suggests that the susceptibility analysis in areas affected by recent strong earthquakes is markedly time-dependent, thus it cannot be performed without carefully subsetting the landslide inventory to account for the time of landslide occurrence. Therefore, to improve the hazard assessment model, we recommend the following: (i) frequent updating of the inventory to be used in the modeling, and (ii) repeated model training and variable set selection to update the susceptibility model and maps.

In addition, we noticed that by employing a postevent TanDEM-X data, the significance of the variable SLO (slope) increased when compared with that obtained using the preevent DEM. This confirms that the susceptibility to further landslides is affected to a significant extent by the changes of topography caused by previous landslides. Consequently, it is appropriate to always use the most recent DEM data for susceptibility mapping (J. Y. Li et al., 2020), especially in contexts in which landslides occur frequently and affect significant portions of the landscape (see Text S7, supporting information). However, the data gaps observed in the TanDEM-X DEM for the whole study area caused by layover and shadow effect hindered us to allow the full potential of this recent DEM. On the other hand, we noticed that the other topographic factors such as ELE, CUR, FAC, TPI, POS, ASP, DAH were not so sensitive to those changes. All this considered, we recommend employing multitemporal high resolution DEMs, if available. However, no systematic collection of such data is available for the entire study area, in our case, as the work of Tang et al. (2019) only covers a small portion of it.

6. Summary and Conclusion

Based on a multitemporal landslide inventory produced after the 2008 Wenchuan Earthquake, we revealed that the controls of postseismic debris remobilizations are evolving rapidly. This implies that susceptibility models relying on a single time-related inventory and a static set of controlling factors and weights may

likely be unreliable, considering the very dynamic nature of the geoenvironment after strong earthquakes. The same applies to susceptibility models trained on cumulative "historical" inventories that collect all the mass displacements within the same sampling set (Text S8 in the supporting information). For postseismic landslide risk assessment and reduction, it is essential to understand for how long a trained susceptibility/hazard model can still be used for successful predictions of postseismic landslides. This study shows that a set of controlling factors determined from a postseismic inventory in a given year may not be suitable for predicting landslides susceptibility already after a few years. This suggests that possible controlling factor evolutions should be carefully assessed when training statistical predictive models, and only time-related observations should be used for sampling. Once recorded, the time of occurrence of new landslide or re-mobilizations can be profitably used to subset time-dependent parameter spaces for multivariate statistical analysis. This is especially true in areas affected by large-magnitude earthquakes, where the methodology and conditioning factors presented in this study could be applied for forecasting the spatial probability of postseismic landslide occurrences, as suggested by the high success rate (AUC) obtained for the immediate postseismic period. Our results also support the need of continued monitoring of channel deposits, from which prolonged threats originate in postearthquake scenarios.

Conflict of Interest

The authors declare no conflicts of interest relevant to this study.

Data Availability Statement

The landslide inventory map data used in this study are archived in a public domain repository https://zenodo.org/record/1484667#.X0iQ4TV5uUk. The NDVI (https://code.earthengine.google.com/5ec9d85ee00478ebb8ea1d8cbcf96519) and TRMM data (https://developers.google.com/earth-engine/datasets/catalog/TRMM_3B43V7) are prepared in Google Earth Engine environment using above codes. Please contact the corresponding author for any questions.

Acknowledgments
This research is financially supported by the Funds for Creative Research Groups of China (Grant No. 41521002), the National Science Fund for Outstanding Young Scholars of China (Grant No. 41622206), and the Fund of SKLGP (SKLGP2019Z002). G. Scaringi acknowledges support by the Fund for International Mobility of Researchers at Charles University (Project No. CZ.02.2.69/0.0/0.0/16_027/0008495, key activity 1-PřF-GEOMOBIL) and the Grant Agency of the Czech Republic (Grant No. 20-28853Y).

References

Alhaj, T. A., Siraj, M. M., Zainal, A., Elshoush, H. T., & Elhaj, F. (2016). Feature selection using information gain for improved structural-based alert correlation. *PLoS One*, *11*(11), e0166017.

Allen, M. P. (1997). The problem of multicollinearity. In M. P. Allen (Ed.), *Understanding regression analysis* (pp. 176–180). Boston, MA: Springer. https://doi.org/10.1007/978-0-585-25657-3_37

Andrews, J., Benisch, M., Sardinha, A., & Sadeh, N. (2007). Using information gain to analyze and fine tune the performance of supply chain trading agents. In J. Collins, P. Faratin, S. D. Parsons, et al. (Eds.), *Agent-mediated electronic commerce and trading agent design and analysis* (pp. 182–199). Springer. https://doi.org/10.1007/978-3-540-88713-3_13

Brocca, L., Ciabatta, L., Massari, C., Moramarco, T., Hahn, S., Hasenauer, S., et al. (2014). Soil as a natural rain gauge: Estimating global rainfall from satellite soil moisture data. *Journal of Geophysical Research: Atmosphere*, *119*(9), 5128–5141. https://doi.org/10.1002/2014JD021489

Carro, M., De Amicis, M., Luzi, L., & Marzorati, S. (2003). The application of predictive modeling techniques to landslides induced by earthquakes: The case study of the 26 September 1997 Umbria–Marche earthquake (Italy). *Engineering Geology*, *69*(1–2), 139–159.

Catani, F., Lagomarsino, D., Segoni, S., & Tofani, V. (2013). Landslide susceptibility estimation by random forests technique: Sensitivity and scaling issues. *Natural Hazards and Earth System Sciences*, *13*(11), 2815–2831.

Chen, M., Tang, C., Xiong, J., Shi, Q. Y., Li, N., Gong, L. F., et al. (2020). The long-term evolution of landslide activity near the epicentral area of the 2008 Wenchuan Earthquake in China. *Geomorphology*, *367*, 107317.

Chen, Y., Wei, Y., Wang, Q., Chen, F., Lu, C., & Lei, S. (2020). Mapping post-earthquake landslide susceptibility: A U-Net like approach. *Remote Sensing*, *12*(17), 2767.

Croissant, T., Steer, P., Lague, D., Davy, P., Jeandet, L., & Hilton, R. G. (2019). Seismic cycles, earthquakes, landslides and sediment fluxes: Linking tectonics to surface processes using a reduced-complexity model. *Geomorphology*, *339*, 87–103.

Dadson, S. J., Hovius, N., Chen, H., Dade, W. B., Lin, J. C., Hsu, M. L., et al. (2004). Earthquake-triggered increase in sediment delivery from an active mountain belt. *Geology*, *32*(8), 733–736. https://doi.org/10.1130/G20639.1

Dahlquist, M P., West, A. J (2019). Initiation and Runout of Post-Seismic Debris Flows: Insights From the 2015 Gorkha Earthquake. *Geophysical Research Letters*, *46*(16), 9658–9668. http://dx.doi.org/10.1029/2019gl083548

Domènech, G., Fan, X., Scaringi, G., van Asch, T. W. J., Xu, Q., Huang, R., & Hales, T. C. (2019). Modelling the role of material depletion, grain coarsening and revegetation in debris flow occurrences after the 2008 Wenchuan earthquake. *Engineering Geology*, *250*, 34–44. https://doi.org/10.1016/j.enggeo.2019.01.010

Domènech, G., Yang, F., Guo, X., Fan, X., Scaringi, G., Dai, L., et al. (2018). Two multi-temporal datasets to track the enhanced landsliding after the 2008 Wenchuan earthquake. Zenodo [Data Set]. https://doi.org/10.5281/zenodo.1405489

Dormann, C. F., Elith, J., Bacher, S., Buchmann, C., Carl, G., Carré, G., et al. (2013). Collinearity: A review of methods to deal with it and a simulation study evaluating their performance. *Ecography*, *36*(1), 27–46.

Dou, J., Yunus, A. P., Bui, D. T., Merghadi, A., Sahana, M., Zhu, Z., et al. (2019). Assessment of advanced random forest and decision tree algorithms for modeling rainfall-induced landslide susceptibility in the Izu-Oshima Volcanic Island, Japan. *Science of the Total Environment*, *662*, 332–346.

Fan, X., Domènech, G., Scaringi, G., Huang, R., Xu, Q., Hales, T. C., et al. (2018b). Spatio-temporal evolution of mass wasting after the 2008 Mw 7.9 Wenchuan earthquake revealed by a detailed multi-temporal inventory. *Landslides*, *15*(12), 2325–2341. https://doi.org/10.1007/s10346-018-1054-5

Fan, X., Scaringi, G., Domènech, G., Yang, F., Guo, X., Dai, L., et al. (2019b). Two multi-temporal datasets that track the enhanced landsliding after the 2008 Wenchuan earthquake. *Earth System Science Data*, *11*(1), 35–55. https://doi.org/10.5194/essd-11-35-2019

Fan, X., Scaringi, G., Korup, O., West, A. J., van Westen, C. J., Tanyas, H., et al. (2019a). Earthquake-induced chains of geologic hazards: Patterns, mechanisms, and impacts. *Reviews of Geophysics*, *57*(2), 421–503. https://doi.org/10.1029/2018RG000626

Fan, R. L., Zhang, L. M., Wang, H. J., & Fan, X. M. (2018a). Evolution of debris flow activities in Gaojiagou Ravine during 2008–2016 after the Wenchuan earthquake. *Engineering Geology*, *235*, 1–10.

Gorum, T., Fan, X., van Westen, C. J., Huang, R., Xu, Q., Tang, C., & Wang, G. (2011). Distribution pattern of earthquake-induced landslides triggered by the 12 May 2008 Wenchuan earthquake. *Geomorphology*, *133*(3–4), 152–167. https://doi.org/10.1016/j.geomorph.2010.12.030

Hall, M. A., & Holmes, G. (2003). Benchmarking attribute selection techniques for discrete class data mining. *IEEE Transactions on Knowledge and Data Engineering*, *15*(6), 1437–1447.

Hovius, N., Meunier, P., Lin, C.-W., Chen, H., Chen, Y.-G., Dadson, S., et al. (2011). Prolonged seismically induced erosion and the mass balance of a large earthquake. *Earth and Planetary Science Letters*, *304*(3–4), 347–355. https://doi.org/10.1016/j.epsl.2011.02.005

Hovius, N., Stark, C. P., & Allen, P. A. (1997). Sediment flux from a mountain belt derived by landslide mapping. *Geology*, *25*(3), 231–234.

Hu, W., Scaringi, G., Xu, Q., & Huang, R. (2018). Internal erosion controls failure and runout of loose granular deposits: Evidence from flume tests and implications for postseismic slope healing. *Geophysical Research Letters*, *45*(11), 5518–5527. https://doi.org/10.1029/2018GL078030

Hu, W., Scaringi, G., Xu, Q., Pei, Z., Van Asch, T. W. J., & Hicher, P.-Y. (2017). Sensitivity of the initiation and runout of flowslides in loose granular deposits to the content of small particles: An insight from flume tests. *Engineering Geology*, *231*, 34–44. https://doi.org/10.1016/j.enggeo.2017.10.001

Jenness, J. (2006). *Topographic position index (TPI) v. 1.2*. Jenness Enterprises.

Keefer, D. K. (1994). The importance of earthquake-induced landslides to long-term slope erosion and slope-failure hazards in seismically active regions. In M. Morisawa (Ed.), *Geomorphology and natural hazards* (pp. 265–284). Elsevier. https://doi.org/10.1016/B978-0-444-82012-9.50022-0

Larsen, I. J., Montgomery, D. R., & Korup, O. (2010). Landslide erosion controlled by hillslope material. *Nature Geoscience*, *3*(4), 247–251. https://doi.org/10.1038/ngeo776

Lee, C. T., Huang, C. C., Lee, J. F., Pan, K. L., Lin, M. L., & Dong, J. J. (2008). Statistical approach to earthquake-induced landslide susceptibility. *Engineering Geology*, *100*(1–2), 43–58.

Lei, S. (2012). A feature selection method based on information gain and genetic algorithm. *2012 International Conference on Computer Science and Electronics Engineering* (Vol. *2*, pp. 355–358). IEEE.

Lin, C.-W., Shieh, C.-L., Yuan, B.-D., Shieh, Y.-C., Liu, S.-H., & Lee, S.-Y. (2004). Impact of Chi-Chi earthquake on the occurrence of landslides and debris flows: Example from the Chenyulan River watershed, Nantou, Taiwan. *Engineering Geology*, *71*(1–2), 49–61. https://doi.org/10.1016/S0013-7952(03)00125-X

Li, J. Y., Wang, W. D., Han, Z., Li, Y., & Chen, G. (2020). Exploring the impact of multitemporal DEM data on the susceptibility mapping of landslides. *Applied Sciences*, *10*, 2518. https://doi.org/10.3390/app10072518

Li, C., Wang, M., & Liu, K. (2018a). A decadal evolution of landslides and debris flows after the Wenchuan earthquake. *Geomorphology*, *323*, 1–12. https://doi.org/10.1016/j.geomorph.2018.09.010

Li, G., West, A. J., Densmore, A. L., Jin, Z., Zhang, F., Wang, J., et al. (2017). Earthquakes drive focused denudation along a tectonically active mountain front. *Earth and Planetary Science Letters*, *472*, 253–265. https://doi.org/10.1016/j.epsl.2017.04.040

Li, G., West, A. J., Densmore, A. L., Jin, Z., Zhang, F., Wang, J., & Hilton, R. G. (2018b). Distribution of earthquake-triggered landslides across landscapes: Towards understanding erosional agency and cascading hazards. In Y. G. Li (Ed.), *Fault-zone guided wave, ground motion, landslide and earthquake forecast* (pp. 160–190). Berlin, Germany and Boston, MA: De Gruyter. https://doi.org/10.1515/9783110543551-170

Marc, O., Hovius, N., & Meunier, P. (2016). The mass balance of earthquakes and earthquake sequences. *Geophysical Research Letters*, *43*(8), 3708–3716. https://doi.org/10.1002/2016GL068333

Marc, O., Hovius, N., Meunier, P., Uchida, T., & Hayashi, S. (2015). Transient changes of landslide rates after earthquakes. *Geology*, *43*(10), 883–886. https://doi.org/10.1130/G36961.1

Martha, T. R., van Westen, C. J., Kerle, N., Jetten, V., & Kumar, K. V. (2013). Landslide hazard and risk assessment using semi-automatically created landslide inventories. *Geomorphology*, *184*, 139–150.

Merghadi, A., Abderrahmane, B., & Tien Bui, D. (2018). Landslide susceptibility assessment at Mila basin (Algeria): A comparative assessment of prediction capability of advanced machine learning methods. *ISPRS International Journal of Geo-Information*, *7*(7), 268.

Merghadi, A., Yunus, A. P., Dou, J., Whiteley, J., ThaiPham, B., Bui, D. T., et al. (2020). Machine learning methods for landslide susceptibility studies: A comparative overview of algorithm performance. *Earth-Science Reviews*, *207*, 103225. https://doi.org/10.1016/j.earscirev.2020.103225

Nowicki Jessee, M. A., Hamburger, M. W., Allstadt, K., Wald, D. J., Robeson, S. M., Tanyas, H., et al. (2018). A global empirical model for near real-time assessment of seismically induced landslides. *Journal of Geophysical Research: Earth Surface*, *123*(8), 1835–1859. https://doi.org/10.1029/2017JF004494

Petley, D. (2019). *Reports of multiple fatal landslides in the Wenchuan area of China*. Retrieved from https://blogs.agu.org/landslideblog/2019/08/22/wenchuan-1/

Quinlan, J. R. (1986). Induction of decision trees. *Machine Learning*, *1*(1), 81–106.

Reichenbach, P., Rossi, M., Malamud, B. D., Mihir, M., & Guzzetti, F. (2018). A review of statistically-based landslide susceptibility models. *Earth-Science Reviews*, *180*, 60–91. https://doi.org/10.1016/j.earscirev.2018.03.001

Segoni, S., Pappafico, G., Luti, T., & Catani, F. (2020). Landslide susceptibility assessment in complex geological settings: Sensitivity to geological information and insights on its parameterization. *Landslides*, *17*, 2443–2453.

Segoni, S., Tofani, V., Rosi, A., Catani, F., & Casagli, N. (2018). Combination of rainfall thresholds and susceptibility maps for dynamic landslide hazard assessment at regional scale. *Frontiers of Earth Science*, *6*, 85.

Shafique, M. (2020). Spatial and temporal evolution of co-seismic landslides after the 2005 Kashmir earthquake. *Geomorphology*, *362*, 107228. http://dx.doi.org/10.1016/j.geomorph.2020.107228
Shen, P., Zhang, L. M., Fan, R., Zhu, H., & Zhang, S. (2020). Declining geohazard activity with vegetation recovery during first ten years after the 2008 Wenchuan earthquake. *Geomorphology*, *352*, 106989.
Shou, K. J., Hong, C. Y., Wu, C. C., Hsu, H. Y., Fei, L. Y., Lee, J. F., & Wei, C. Y. (2011). Spatial and temporal analysis of landslides in Central Taiwan after 1999 Chi-Chi earthquake. *Engineering Geology*, *123*(1–2), 122–128. https://doi.org/10.1016/j.enggeo.2011.03.014
Slaymaker, O. (2010). Mountain hazards. In I. Alcántara-Ayala & A. Goudie (Eds.), *Geomorphological Hazards and Disaster Prevention*, (pp. 33–48). Cambridge, MA: Cambridge University Press.
Tang, C., Tanyas, H., van Westen, C. J., Tang, C., Fan, X., & Jetten, V. G. (2019). Analysing post-earthquake mass movement volume dynamics with multi-source DEMs. *Engineering Geology*, *248*, 89–101.
Tang, C., Van Westen, C. J., Tanyas, H., & Jetten, V. G. (2016). Analysing post-earthquake landslide activity using multi-temporal landslide inventories near the epicentral area of the 2008 Wenchuan earthquake. *Natural Hazards and Earth System Sciences*, *16*(12), 2641–2655. https://doi.org/10.5194/nhess-16-2641-2016
Tang, C., Zhu, J., Ding, J., Cui, X. F., Chen, L., & Zhang, J. S. (2011). Catastrophic debris flows triggered by a 14 August 2010 rainfall at the epicenter of the Wenchuan earthquake. *Landslides*, *8*(4), 485–497. https://doi.org/10.1007/s10346-011-0269-5
Tian, Y., Owen, L. A., Xu, C., Ma, S., Li, K., Xu, X., et al. (2020). Landslide development within 3 years after the 2015 M w 7.8 Gorkha earthquake, Nepal. *Landslides*, *17*, 1251–1267.
van Westen, C. J., Castellanos, E., & Kuriakose, S. L. (2008). Spatial data for landslide susceptibility, hazard, and vulnerability assessment: An overview. *Engineering Geology*, *102*(3–4), 112–131.
Wang, W., Godard, V., Liu-Zeng, J., Scherler, D., Xu, C., Zhang, J., et al. (2017). Perturbation of fluvial sediment fluxes following the 2008 Wenchuan earthquake: Fluvial sediment fluxes following large-magnitude earthquake. *Earth Surface Processes and Landforms*, *42*(15), 2611–2622. https://doi.org/10.1002/esp.4210
Xu, C., Xu, X., Yao, X., & Dai, F. (2014). Three (nearly) complete inventories of landslides triggered by the May 12, 2008 Wenchuan Mw 7.9 earthquake of China and their spatial distribution statistical analysis. *Landslides*, *11*(3), 441–461. https://doi.org/10.1007/s10346-013-0404-6
Xu, Q., Zhang, S., Li, W., & Van Asch, T. W. (2012). The 13 August 2010 catastrophic debris flows after the 2008 Wenchuan earthquake, China. *Natural Hazards and Earth System Sciences*, *12*, 201–216.
Yang, W., Qi, W., Wang, M., Zhang, J., & Zhang, Y. (2017). Spatial and temporal analyses of post-seismic landslide changes near the epicentre of the Wenchuan earthquake. *Geomorphology*, *276*, 8–15. https://doi.org/10.1016/j.geomorph.2016.10.010
Yang, W., Qi, W., & Zhou, J. (2018). Decreased post-seismic landslides linked to vegetation recovery after the 2008 Wenchuan earthquake. *Ecological Indicators*, *89*, 438–444. https://doi.org/10.1016/j.ecolind.2017.12.006
Yokoyama, R., Shirasawa, M., & Pike, R. J. (2002). Visualizing topography by openness: A new application of image processing to digital elevation models. *Photogrammetric Engineering & Remote Sensing*, *68*(3), 257–266.
Yunus, A. P., Dou, J., Song, X., & Avtar, R. (2019). Improved bathymetric mapping of coastal and lake environments using Sentinel-2 and Landsat-8 images. *Sensors*, *19*(12), 2788.
Yunus, A. P., Fan, X., Tang, X., Jie, D., Xu, Q., & Huang, R. (2020). Decadal vegetation succession from MODIS reveals the spatio-temporal evolution of post-seismic landsliding after the 2008 Wenchuan earthquake. *Remote Sensing of Environment*, *236*, 111476.
Zhang, S., & Zhang, L. M. (2017). Impact of the 2008 Wenchuan earthquake in China on subsequent long-term debris flow activities in the epicentral area. *Geomorphology*, *276*, 86–103. https://doi.org/10.1016/j.geomorph.2016.10.009
Zhang, S., Zhang, L., Lacasse, S., Nadim, F. (2016). Evolution of Mass Movements near Epicentre of Wenchuan Earthquake, the First Eight Years. *Scientific Reports*, *6*(1). http://dx.doi.org/10.1038/srep36154

References From the Supporting Information

Böhner, J., & Antonić, O. (2009). Land-surface parameters specific to topo-climatology. *Developments in Soil Science*, *33*, 195–226.
Budimir, M. E. A., Atkinson, P. M., & Lewis, H. G. (2015). A systematic review of landslide probability mapping using logistic regression. *Landslides*, *12*(3), 419–436. https://doi.org/10.1007/s10346-014-0550-5
Guisan, A., Weiss, S. B., & Weiss, A. D. (1999). GLM versus CCA spatial modeling of plant species distribution. *Plant Ecology*, *143*(1), 107–122. https://doi.org/10.1023/A:1009841519580
Martelloni, G., Segoni, S., Fanti, R., & Catani, F. (2012). Rainfall thresholds for the forecasting of landslide occurrence at regional scale. *Landslides*, *9*(4), 485–495. https://doi.org/10.1007/s10346-011-0308-2
Melton, M. A. (1965). The geomorphic and paleoclimatic significance of alluvial deposits in southern Arizona. *The Journal of Geology*, *73*(1), 1–38. https://doi.org/10.1086/627044
Tape, T. G. (2019). *The area under an ROC curve*. Interpreting Diagnostic Tests, University of Nebraska Medical Center. Retrieved from http://gim.unmc.edu/dxtests/roc3.htm
Tarboton, D. G. (1997). A new method for the determination of flow directions and upslope areas in grid digital elevation models. *Water Resources Research*, *33*(2), 309–319. https://doi.org/10.1029/96WR03137
Uğuz, H. (2011). A two-stage feature selection method for text categorization by using information gain, principal component analysis and genetic algorithm. *Knowledge-Based Systems*, *24*(7), 1024–1032.